REGULAR ARTICLE

Assessment of higher-order spin–orbit effects on electronic g-tensors of d^1 transition-metal complexes by relativistic two- and four-component methods

Peter Hrobárik · Michal Repiský ·
Stanislav Komorovský · Veronika Hrobáriková ·
Martin Kaupp

Abstract The electronic g-tensors of a series of V, Cr, Mo, W, Tc, and Re d^1 transition-metal complexes have been studied systematically by density functional theory (DFT) methods. The comparison between one-component second-order perturbation theory calculations with two- and four-component first-order perturbation calculations has allowed an assessment of the importance of higher-order spin-orbit contributions. Using an efficient matrix Dirac–Kohn–Sham implementation with relativistic kinetic balance basis sets, it has been possible for the first time to apply four-component DFT also to g-tensors of larger models for biological vanadium, molybdenum, and tungsten metal sites. Higher-order spin–orbit effects are generally crucial for an accurate determination of the g-tensors in such complexes, in many cases more important than the choice of non-hybrid or hybrid density functional. A systematic scaling analysis of the spin–orbit integrals shows that second-order spin–orbit effects may be of the same size as the leading first-order effects and thus alter the computed g-tensors fundamentally, in particular for the $5d$ species. In the latter case, even third-order effects may be non-negligible.

Keywords Biological transition-metal sites · Density functional theory (DFT) · Dirac–Kohn–Sham method · Douglas–Kroll–Hess Hamiltonian · Electron paramagnetic resonance (EPR) · g-Tensor · Relativistic effects · Spin–orbit coupling · Transition-metal complexes

P. Hrobárik · V. Hrobáriková · M. Kaupp (✉)
Technische Universität Berlin, Institut für Chemie,
Theoretische Chemie, Sekr. C7, Strasse des 17. Juni 135,
10623 Berlin, Germany
e-mail: martin.kaupp@tu-berlin.de

P. Hrobárik (✉) · M. Repiský · S. Komorovský
Institute of Inorganic Chemistry, Slovak Academy of Sciences,
Dúbravská cesta 9, 84536 Bratislava, Slovakia
e-mail: peter.hrobarik@savba.sk

M. Repiský
Department of Chemistry,
Centre for Theoretical and Computational Chemistry (CTCC),
University of Tromsø, 9037 Tromsø, Norway

1 Introduction

The electronic g-tensor is a central parameter of electron paramagnetic resonance (EPR) spectroscopy [1, 2]. Moreover, it is dominated by spin–orbit coupling (SOC) and thus viewed as a fundamentally relativistic property. Recent progress in high-field EPR spectroscopy has put the g-tensor further into the focus of interest, and accurate quantum-chemical calculations of g-tensors, taking all intrinsic, dynamic, and environmental effects into account, have become an important topic in quantum chemistry [3]. Such calculations do in turn help significantly to interpret and analyze EPR spectra, and they may contribute to structure elucidation. In particular, the study of the active sites of metalloenzymes is of central interest, and the presence of $3d$ all the way to $5d$ transition-metal centers places substantial demands on computational studies of g-tensors [4–9]. The proper treatment of spin–orbit effects is crucial for a reliable prediction/interpretation of the data. In this respect, computational methods for obtaining g-tensors may be divided into those that treat SOC by perturbation theory (based on a scalar relativistic or non-relativistic wavefunction) and those that include SOC already in the zeroth-order wave function. In the former

case, the inclusion of SOC is usually restricted to the leading (first) order in perturbation theory, that is to $\hat{O}(\alpha^2)$ in the fine structure constant α [10–13] [see refs. [14, 15] for perturbation approaches including relativistic terms up to $\hat{O}(\alpha^4)$], whereas quasirelativistic two-component and fully relativistic four-component calculations include SOC to all orders. A few comparison studies of one- and two-component result on a number of linear heavy-element di- and triatomics, on cysteine radical, and on a few small transition-metal complexes, have already pointed out the importance of higher-order SOC effects for the g-tensors of (1) systems containing heavy elements and thus exhibiting large SOC, and (2) systems with near-degeneracy of energy levels at the non-relativistic level, where SOC is thus also large on a relative scale [16].

In motivating their $\hat{O}(\alpha^4)$ quadratic response formalism based on non-relativistic Kohn–Sham wavefunctions, Rinkevicius et al. [14] have still recently deplored that two-component calculations of g-tensors have so far been restricted only to a few relatively small systems, with the exception of van Lenthe's implementation of the zero-order regular approximation (ZORA) [17], which, however, neglects spin polarization and is limited to doublet states only. One purpose of the present work is to show that, by using a recently reported efficient implementation of the matrix Dirac–Kohn–Sham methodology [18–20], even four-component spin-polarized DFT calculations of g-tensors are now applicable to transition-metal complexes up to about 50–100 atoms.

The second goal of the present work is to find out up to what perturbation order SOC effects are relevant for the g-tensor. A comparison of one-component second-order perturbation calculations with two- or four-component calculations will provide only the overall amount of SOC effects beyond the leading-order treatment. However, based on a scaling of the prefactors of the spin–orbit integrals in two-component calculations and a fit of polynomials to the dependence of computed g-tensor components on the scaling factor, we have previously analyzed the contributing perturbation orders for diatomics [16]. Here, we extend these analyses to chemically more relevant sizes of transition-metal complexes.

2 Computational details

The structures of all square-pyramidal complexes were optimized at the unrestricted BP86/TZVP level of theory (without inclusion of spin–orbit coupling) with the TURBOMOLE 6.0 program package [21]. In order to speed up the computations, the Coulomb term was approximated by the resolution of the identity (RI) method, using TZVP auxiliary basis sets [22]. Quasirelativistic energy-adjusted

small-core Stuttgart-type effective-core pseudopotentials with corresponding $(7s6p5d)/[5s3p3d]$ and $(7s6p5d)/[6s3p3d]$ GTO valence basis sets were used for the 4d and 5d metal centers, respectively [23]. Triple-zeta all-electron basis sets, denoted as def-TZVP, were employed for all other atoms [24]. The optimized structures of the first three larger complexes ([V(hidpa)$_2$]$^{2-}$, denoted as amavadin throughout this work, [MoO$_2$L^1]$^-$, and [MoO$_2$L^2]$^-$) have been taken from Refs. [25] and [6], respectively. The structures of two related metallodithiolene scorpionate complexes [MS(Tp){S$_2$C$_2$(CO$_2$Me)$_2$}] (M = Mo, W) have been fully optimized at the RI-BP86/TZVP level, starting from the crystal structure reported in Ref. [26].

All SCF and property calculations have been carried out at the Kohn–Sham DFT level with the ReSpect-MAG code [27], including a new four-component module [28]. Calculations have been done either at the generalized gradient approximation (GGA) level, with the Becke exchange and Perdew correlation functionals (BP86) [29–31], and in the case of one- and two-component calculations also employing Becke's three-parameter hybrid functional with Perdew–Wang GGA correlation (B3PW91) [32–35]. As in our previous studies on EPR parameters of transition-metal complexes, the best agreement with experimental data for both hyperfine and g-tensors was obtained with hybrid functionals incorporating approximately 30–40% Hartree–Fock exchange [5, 6, 36], we have also evaluated the use of one-parameter BPW91-based functionals of the general form $E_{XC}^{hybrid} = a_0 E_X^{HF} + (1 - a_0)E_X^{B88} + E_C^{PW91}$, with a_0 indicating the amount of Hartree–Fock exact exchange (chosen as 0.30, 0.40, and 0.50 in the following denoted as BPW91-30HF, BPW91-40HF, and BPW91-50HF). All calculations, except those at the four-component level, were performed without fitting of electron and spin densities. An integration grid of 128 radial shells and fine angular quadrature corresponding to about 11000 grid points per atom has been employed. All-electron Hirao basis sets of the quality $(20s15p9d)$, $(21s19p12d)$, and $(23s23p15d10f)$ were used for the 3d, 4d, and 5d metal centers, respectively [37]. A corresponding basis set of the quality $(20s15p9d)$ was employed for bromine. All other ligand atoms were treated by uncontracted Huzinaga–Kutzelnigg-type IGLO-II basis sets [38].

One-component g-tensor calculations with second-order perturbational treatment of SOC were performed using the approach described in Refs. [13, 16]. The ground-state, second-order transformed Douglas–Kroll–Hess (DKH) wave function was used to account for scalar relativistic effects. Accordingly, the spin–orbit integrals were calculated perturbationally in the atomic mean-field (AMFI) approximation [39] at first-order DKH level. In this treatment, we did not account for the transformation of the Zeeman operator, since this is much less important than the transformation of the SOC operator.

The two-component calculations of g-tensors were done with our previously described non-collinear spin-density two-component approach, as implemented in the ReSpect-MAG code [16]. It is important to note that our method includes spin polarization in contrast to restricted two-component implementations such as described in Refs. [17, 40]. Here, the Kohn–Sham (KS) molecular orbitals φ_i are considered as a linear combination of atomic orbitals χ_λ with complex coefficients $C^\sigma_{\lambda i}$ ($\sigma = \alpha, \beta$),

$$\varphi_i = \begin{pmatrix} \sum_\lambda C^\alpha_{\lambda i} \chi_\lambda \\ \sum_\lambda C^\beta_{\lambda i} \chi_\lambda \end{pmatrix}. \tag{1}$$

The use of a two-component method allows the description of an arbitrary orientation of electron spin (or magnetic moment $\vec{m}$ in the presence of SOC), in contrast to the collinear one-component approach, where the spin direction is fixed along the z axis. The components of the g-tensor were obtained from three spin-unrestricted two-component DFT self-consistent-field (SCF) procedures with orthogonal orientations of $\vec{m}(m_1, m_2, m_3)$ as the derivatives of the energy with respect to the magnetic field [16, 41]:

$$E(m_v, B_u) \approx E_0(m_v) + B_u \cdot \frac{1}{2c} g_{uv}(m_v) \cdot \tilde{S}_v$$
$$\Rightarrow g_{uv} = \frac{2c}{\tilde{S}_v} \frac{\partial E(m_v, B_u)}{\partial B_u} \quad (u, v = 1, 2, 3) \tag{2}$$

where $\tilde{S}$ is the effective spin of the system (i.e., the spin that would characterize the system in the absence of SO effects). The principal axes in small square-pyramidal $[MOX_4]^q$ complexes are known a priori and thus their choice is trivial. Coordinates of atoms in larger complexes were transformed in such a way that new x, y, and z axes were placed along the principal axes of the g-tensor obtained at one-component DKH level. At these coordinates, one-component DKH density matrices were taken as initial guess. By orienting the initial spin successively along these axes allowed convergence of all systems to the states with magnetic moments oriented along principal axes of the g-tensor (the latter were evaluated by the values of off-diagonal elements of the g-matrix). Note that different total energies are obtained for the three different orientations of the magnetic moment. The calculations used the quasirelativistic Douglas–Kroll–Hess (DKH) Hamiltonian, with transformation of the scalar relativistic part to second order and variational use of the atomic meanfield approximation (using the AMFI program) for the spin–orbit integrals up to first DKH order.

Four-component calculations of the electronic g-tensor were carried out in the matrix Dirac–Kohn–Sham framework using a restricted kinetically balanced basis set for the small component (mDKS-RKB method) [19]. Here, the KS molecular orbitals are expanded as

$$\varphi_i^{L(m_v,0)} = \sum_\lambda C_{\lambda i}^{L(m_v,0)} \chi_\lambda$$
$$\varphi_i^{S(m_v,0)} = \sum_\lambda C_{\lambda i}^{S(m_v,0)} \frac{1}{2c} \vec{\sigma} \cdot \vec{p} \chi_\lambda \tag{3}$$

where χ_λ is the λth basis function (even and odd λ indices represent alpha and beta spinors, respectively), c is the speed of light, $\vec{p}$ is the momentum operator, the vector $\vec{\sigma} = (\sigma_1, \sigma_2, \sigma_3)$ is composed of the three Pauli matrices

$$\sigma_1 = \begin{pmatrix} 0 & 1 \\ 1 & 0 \end{pmatrix} \quad \sigma_2 = \begin{pmatrix} 0 & -i \\ i & 0 \end{pmatrix} \quad \sigma_3 = \begin{pmatrix} 1 & 0 \\ 0 & -1 \end{pmatrix}, \tag{4}$$

and $C_{\lambda i}^{L(m_v,0)}$ and $C_{\lambda i}^{S(m_v,0)}$ represent the expansion coefficients for the large and the small component, respectively, for a system with magnetic moment vector $\vec{m}$ oriented along the v axis. The final expression for the g-tensor within the mDKS-RKB approach can be written as

$$g_{uv} = \frac{1}{\tilde{S}_v} \left(\mathbf{C}_{(i)}^{L(m_v,0)\dagger} \ \mathbf{C}_{(i)}^{S(m_v,0)\dagger} \right) \begin{pmatrix} \mathbf{0} & \Lambda_{B_u}^{P\dagger} \\ \Lambda_{B_u}^P & \mathbf{0} \end{pmatrix} \begin{pmatrix} \mathbf{C}_{(i)}^{L(m_v,0)} \\ \mathbf{C}_{(i)}^{S(m_v,0)} \end{pmatrix}, \tag{5}$$

where

$$\left(\Lambda_{B_u}^P \right)_{\lambda\tau} \equiv \frac{1}{2} \langle \chi_\lambda | \vec{\sigma} \cdot \vec{p} \{ (\vec{r} - \vec{r}_0) \times \vec{\sigma} \}_u | \chi_\tau \rangle \tag{6}$$

and $\vec{r}_0$ is an arbitrary fixed gauge origin. In the present work, we consider only a common gauge origin positioned at the unique heavy metal center. This has been shown previously to be a good choice. Since the MO coefficients do not depend on the external uniform magnetic field $\vec{B}$, they can be obtained using three unperturbed SCF calculations for the three orientations of the magnetic moment vector corresponding to the principal axes of the g-tensor. Computation of the expression (5) in this manner is straightforward and takes only a negligible fraction of the SCF computation time as one may expect from the calculation of a first-order property. Furthermore, it has to be noted that all g-tensor computations were done with a finite-size nucleus model employing the Gaussian charge distribution.

As all calculations are carried out within the same program package, using identical basis sets, exchange–correlation potentials, and integration grids, a particularly straightforward comparison of these methods is possible. There is one caveat to this statement: the AMFI spin–orbit operators used in our one- and two-component calculations include the so-called spin-other-orbit (SOO) term resulting from the relativistic Breit term of electron–electron

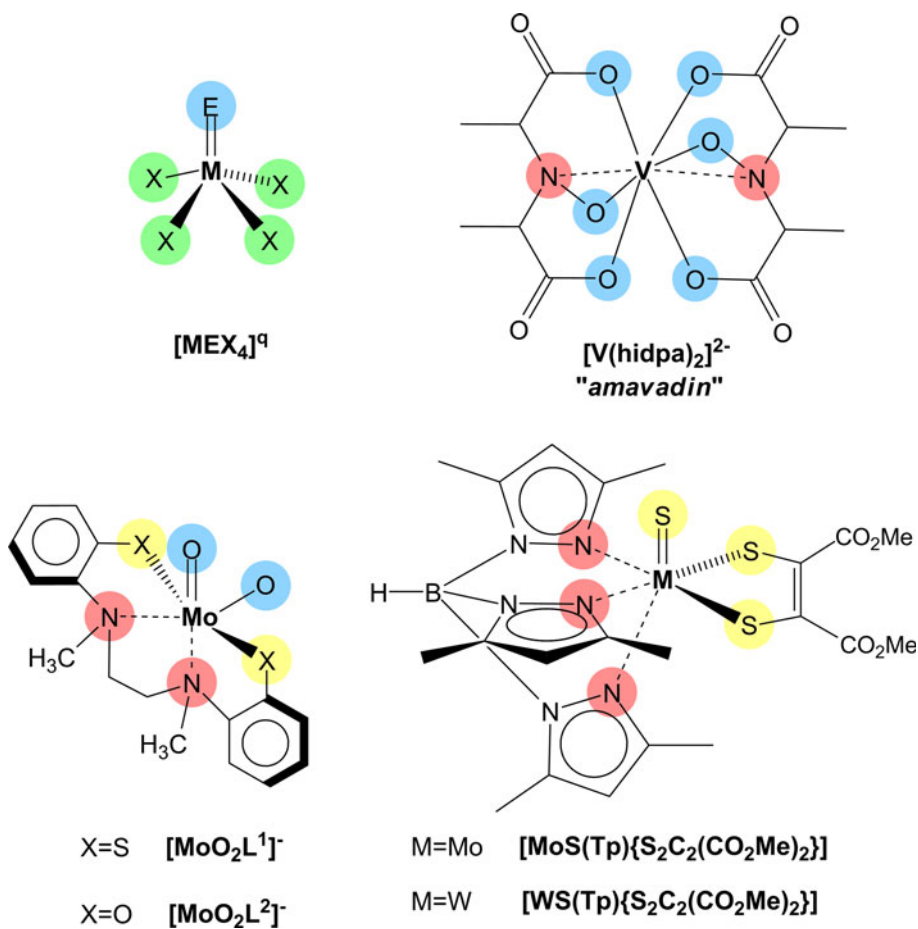**Table 1** Computed g-tensor principal values for d^1 transition-metal complexes of the type MOX_4^q

Compound	Method	BP86			B3PW91		
		$g_\parallel$ [ppt]	$g_\perp$ [ppt]	g_{iso} [ppt]	$g_\parallel$ [ppt]	$g_\perp$ [ppt]	g_{iso} [ppt]
$[VOCl_4]^{2-}$	DKH-1comp	−13	−16	−14	−28	−23	−25
	DKH-2comp	−17	−19	−18	−29	−24	−26
	mDKS-4comp	−23	−22	−22			
	Exp.	−54	−23	−33	−54	−23	−33
$[CrOCl_4]^-$	DKH-1comp	18	−17	−6	13	−29	−15
	DKH-2comp	16	−21	−9	12	−30	−16
	mDKS-4comp	16	−25	−12			
	Exp.	−10	−25	−20	−10	−25	−20
$[MoOF_4]^-$	DKH-1comp	−65	−54	−58	−83	−66	−71
	DKH-2comp	−80	−66	−70	−93	−70	−78
	mDKS-4comp	−85	−71	−76			
	Exp.	−107	−77	−87	−107	−77	−87
$[MoOCl_4]^-$	DKH-1comp	0	−43	−29	−12	−53	−39
	DKH-2comp	−9	−52	−38	−19	−57	−44
	mDKS-4comp	−11	−57	−42			
	Exp.	−37	−55	−49	−37	−55	−49
$[MoNCl_4]^{2-}$	DKH-1comp	−57	−9	−25	−90	−14	−39
	DKH-2comp	−68	−15	−33	−94	−19	−44
	mDKS-4comp	−78	−17	−37			
	Exp.	−96	−18	−44	−96	−18	−44
$[TcNF_4]^-$	DKH-1comp	−48	−15	−26	−68	−17	−34
	DKH-2comp	−58	−22	−34	−74	−23	−40
	mDKS-4comp	−60	−23	−36			
	Exp.	−107	−12	−44	−107	−12	−44
$[TcNCl_4]^-$	DKH-1comp	40	5	17	34	3	13
	DKH-2comp	35	0	12	30	−3	8
	mDKS-4comp	37	0	12			
	Exp.	6	−2	1	6	−2	1
$[TcNBr_4]^-$	DKH-1comp	197	65	109	212	47	102
	DKH-2comp	174	55	94	191	38	89
	mDKS-4comp	178	55	96			
	Exp.	145	32	70	145	32	70
$[WOF_4]^-$	DKH-1comp	−277	−178	−211	−331	−208	−249
	DKH-2comp	−381	−243	−289	−412	−251	−305
	mDKS-4comp	−389	−250	−296			
	Exp.	−403	−330	−354	−403	−330	−354
$[WOCl_4]^-$	DKH-1comp	−96	−144	−128	−140	−169	−159
	DKH-2comp	−161	−206	−191	−195	−217	−210
	mDKS-4comp	−173	−215	−201			
	Exp.	−212	−252	−239	−212	−252	−239
$[WOBr_4]^-$	DKH-1comp	32	−130	−76	−2	−158	−106
	DKH-2comp	−24	−186	−132	−52	−200	−151
	mDKS-4comp	−30	−196	−141			
	Exp.	−99	−206	−170	−99	−206	−170

Table 1 continued

Compound	Method	BP86			B3PW91		
		$g_\parallel$ [ppt]	$g_\perp$ [ppt]	g_{iso} [ppt]	$g_\parallel$ [ppt]	$g_\perp$ [ppt]	g_{iso} [ppt]
[ReOCl$_4$]	DKH-1comp	76	−143	−70	77	−161	−82
	DKH-2comp	16	−209	−134	20	−216	−138
	mDKS-4comp	13	−217	−141			
	Exp.	−28	−294	−205	−28	−294	−205
[ReOBr$_4$]	DKH-1comp	259	−109	13	297	−131	11
	DKH-2comp	197	−169	−47	233	−181	-43
	mDKS-4comp	203	−178	−51			
	Exp.	168	−237	−102	168	−237	−102
[ReNCl$_4$]$^-$	DKH-1comp	−8	−17	−14	−47	−23	−31
	DKH-2comp	−46	−69	−61	−79	−75	−76
	mDKS-4comp	−54	−72	−66			
	Exp.	−88	−57	−67	−88	−57	−67
[ReNBr$_4$]$^-$	DKH-1comp	162	31	75	144	17	59
	DKH-2comp	117	−19	26	102	−33	12
	mDKS-4comp	118	−21	25			
	Exp.	67	−29	3	67	−29	3

Experimental data as compiled in ref. [42]

Fig. 1 Schematic structures of the d^1 transition-metal complexes studied in this work

[MEX$_4$]^q

[V(hidpa)$_2$]$^{2-}$ "amavadin"

X=S [MoO$_2$L^1]$^-$

X=O [MoO$_2$L^2]$^-$

M=Mo [MoS(Tp){S$_2$C$_2$(CO$_2$Me)$_2$}]

M=W [WS(Tp){S$_2$C$_2$(CO$_2$Me)$_2$}]

interaction. Moreover, the direct use of the Kohn–Sham wavefunction to compute the SOC integrals introduces also an exchange-like term to the spin-same-orbit (SSO) contribution [13]. Currently, the four-component implementation starts from the Dirac-Coulomb Hamiltonian and thus neglects the Breit interaction and the resulting SOO term. As the effective Kohn–Sham potential is used to compute the two-electron SOC contributions, the abovementioned exchange-like contributions are also absent. Previous experience indicates that the SOO and exchange-like terms diminish the overall SOC interactions somewhat. On a relative scale, this reduction is more pronounced for lighter atoms than for heavier ones. The lightest central atoms contributing dominantly to SOC interactions in the present complexes are $3d$ elements. We have found previously at the one-component perturbation level, that the SOO term corresponds to about 12% of the overall two-electron SOC contributions and the missing exchange-like term another 6% [13]. We expect thus, that the SOC treatment of the present four-component treatment will underestimate the two-electron SOC terms by about 18%. As the two-electron terms are about 55% of the one-electron terms in absolute magnitude (but opposite in sign) [13], this suggests a resulting overestimate of SOC matrix elements by about 10% for $3d$ complexes. For heavier central atoms, both the relative importance of the SOO and exchange-like terms to two-electron SOC and the relative magnitude of two-electron compared to one-electron SOC are significantly reduced. We expect thus the largest relative deviations between two-component and four-component results for the vanadium and chromium complexes of the present study. This should be kept in mind when assessing the influence of higher-order SOC effects for the g-tensors of the $3d$ complexes.

3 Results and discussion

Axial d^1 [MEX$_4$]^q complexes (M = V, Cr, Mo, Tc, W, Re; E = O, N; X = F, Cl, Br; q = 0,−1,−2). The electronic g-tensors in these smaller square-pyramidal transition-metal complexes have already been studied extensively at the second-order perturbation one-component level [11, 42]. We have so far found indications of the importance of higher-order SOC effects on g-tensors in two-component calculations for a number of smaller Mo(V) and W(V) systems including [MO(bdt)$_2$]$^−$ (bdt = benzene-1,2-dithiolate), [MOCl$_5$]$^{2−}$, and [MOCl$_4$]$^−$ (M = Mo, W) [4, 5]. Results for the latter two complexes are now extended to a more systematic survey of one-, two, and four-component data for a series of valence-isoelectronic group 5–7 $3d$, $4d$, and $5d$ complexes (Table 1; Figs. 1, 2). As the four-component calculations are so far limited to non-hybrid

functionals, the comparison between the one-, two-, and four-component calculations is done at BP86 level.

As is apparent particularly from Fig. 2, the inclusion of only first-order SOC at one-component level provides in most cases appreciably too high g-shift tensor components (too positive or insufficiently negative). These values are lowered significantly, and agreement with experiment is thus improved systematically, at two- and four-component levels. Notably, the two-component DKH and four-component mDKS results agree closely, as has been found also in an initial evaluation of the mDKS approach for a few small complexes [19]. Thus, obviously, higher-order SOC effects are important here for the entire series of complexes in Table 1, Fig. 2 and they are reproduced with similar accuracy at two- and four-component levels. In most cases, the overestimate at
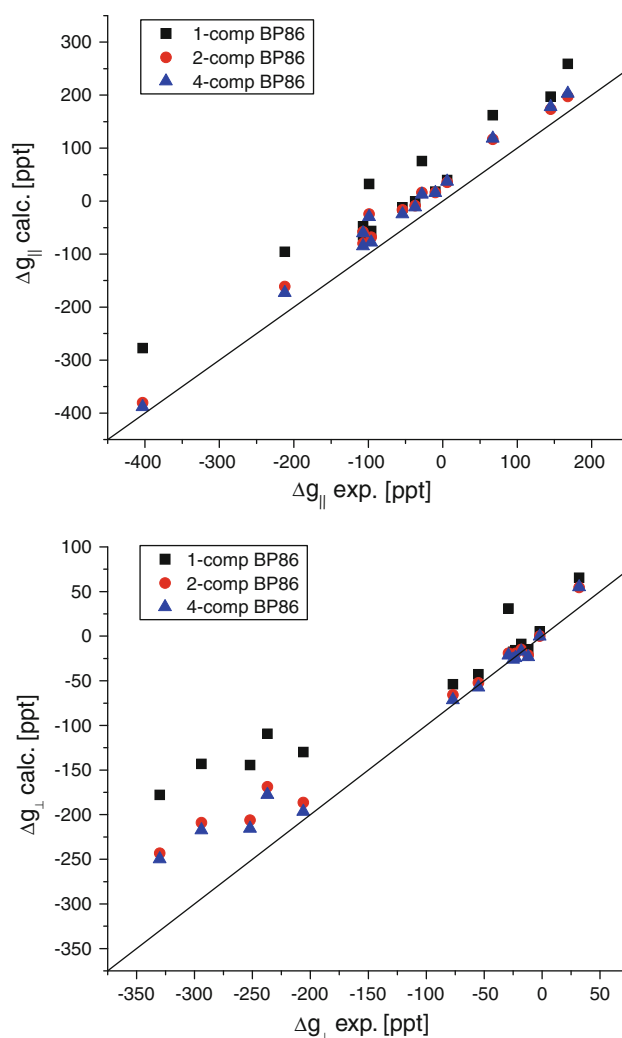

Fig. 2 Comparison of the computed g-shift tensor components (BP86 results in ppt) by one-, two-, and four-component approaches with experiment for the [MOX$_4$]^q series
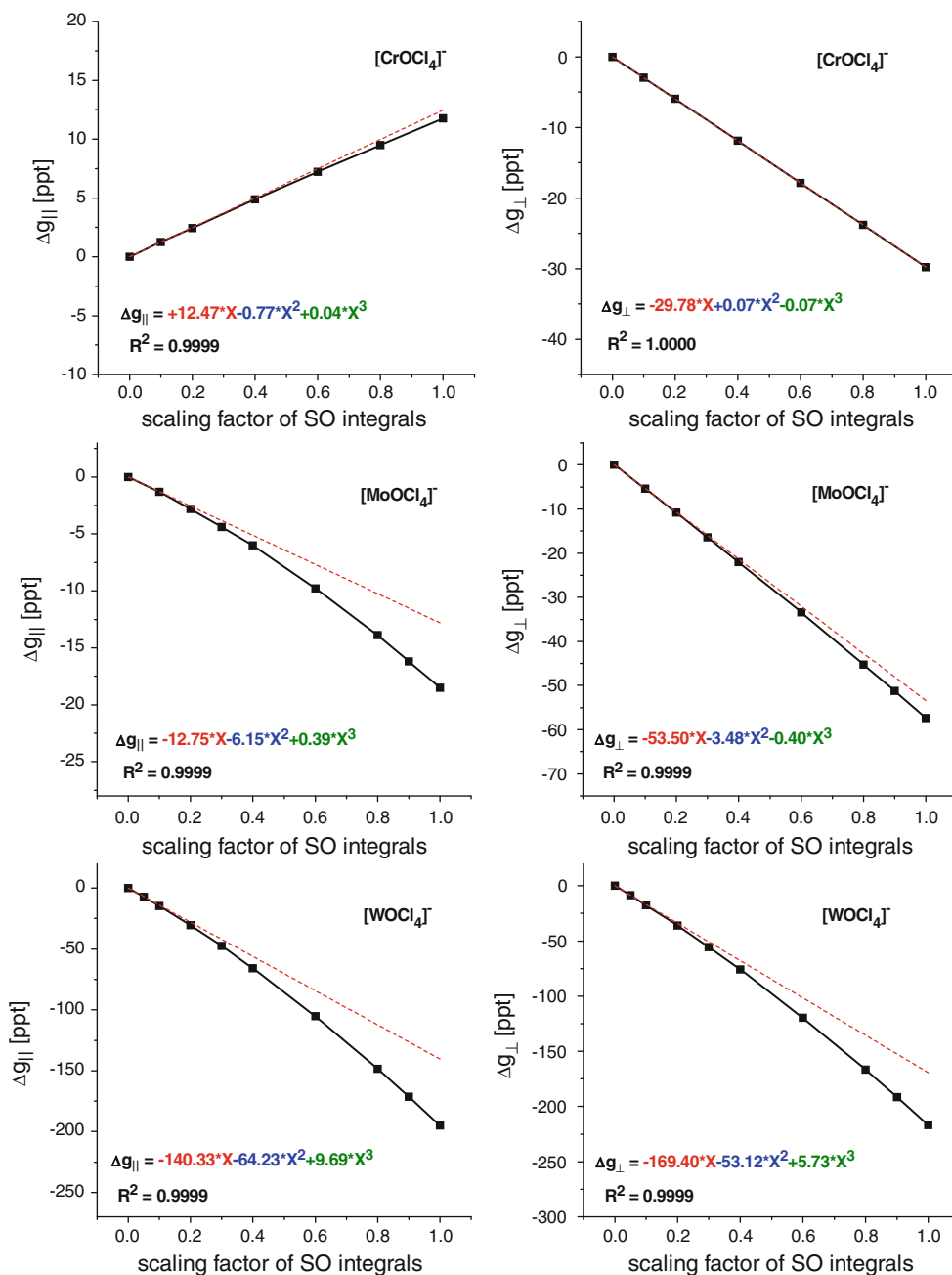
Fig. 3 Dependence of the g-shift tensor components in $[M^VOCl_4]^-$ (M = Cr, Mo, W) complexes on the scaling of spin–orbit integrals. B3PW91 results at two-component DKH level. The *red dashed line* corresponds to the second-order perturbational treatment, which includes only first-order SOC effects

one-component level is more pronounced for $\Delta g_{\|}$ than for $\Delta g_{\perp}$ (the only exceptions are WOF_4^- and $ReOX_4$), and it increases notably from 4d to 5d systems. For instance, going across the series $CrOCl_4^- \rightarrow MoOCl_4^- \rightarrow WOCl_4^-$, the differences are 28 ppt, 37 pt, and 116 ppt, respectively, for $\Delta g_{\|}$ and 8 ppt, 12 pt, and 108 ppt, respectively, for $\Delta g_{\perp}$ (Table 1).

The largest relative difference between two- and four-component results is seen for the vanadium and chromium complexes, in agreement with the largest relative importance of differences in the treatment of two-electron SOC terms (see Sect.2). As for 3d complexes, the SOC matrix elements of the four-component calculations may be about 10% too large compared to the two-component results, the first-order SOC contributions will be overestimated by 10%, and the second-order SOC terms by roughly 20%. This is consistent with the direction and approximate magnitude of the overall differences.

The dependence of the SOC contributions on the perturbation level is evaluated graphically at the two-component level by SOC scaling analyses for a few pertinent complexes in Figs. 3, 4 (see ref. [16] for similar analyses of some diatomics). Already, the visual inspection of the results shows clearly that the dependence of both $\Delta g_\parallel$ and $\Delta g_\perp$ on the scaling factor of the SOC integrals in the two-component calculations displays appreciable curvature, and terms linear in SO coupling are not sufficient to describe the behavior in systems containing heavier atoms. The dashed straight line gives the linear term only, which we have found previously to reproduce faithfully the g-shift components obtained in one-component calculations with second-order perturbation theory. Fitting of the curves by a polynomial up to third order underlines the dominance of first- and second-order terms and the general significance of the latter. Interestingly, however, even third-order SOC contributions, which are roughly one or two orders of magnitude smaller than the second-order ones, become non-negligible for an accurate description of the g-tensors of the 5d complexes. The quadratic prefactor (associated with second-order SOC effects) increases with principal quantum number and reaches the same order of magnitude as the linear prefactor for the 5d systems (and already for

the $\Delta g_\parallel$ component of the 4d complex [MoOCl$_4$]$^-$). That is, in these cases, g-shift components obtained with a leading-order perturbation treatment will exhibit errors on the order of 50–100%. In fact, for [ReNCl$_4$]$^-$, the quadratic prefactor of the $\Delta g_\perp$ component even clearly exceeds the linear one and thus the relative errors in the g-shift components are particularly dramatic for a one-component treatment (cf. Fig. 4). A comparison of the differences between one-component and multi-component methods for analogous complexes of neighboring metal atoms (Mo vs. Tc, W vs. Re) indicates a comparable size of the higher-order SOC effects in the same row of the periodic table. And while the contributions beyond the leading linear SOC term for 3d metal complexes are smaller in absolute values than for their 4d or 5d congeners, they can clearly be non-negligible on a relative scale (see also below for amavadin).

The dependence of the accuracy on the exchange–correlation functional is evaluated in Fig. 5 at two-component level for the same complexes studied in Table 1, and a larger number of functionals is evaluated in Table 2 for two selected complexes. Inclusion of Hartree–Fock exchange improves particularly the results for $\Delta g_\parallel$. However, when comparing Figs. 2 and 5, it is obvious that inclusion of higher-order SOC terms is much more
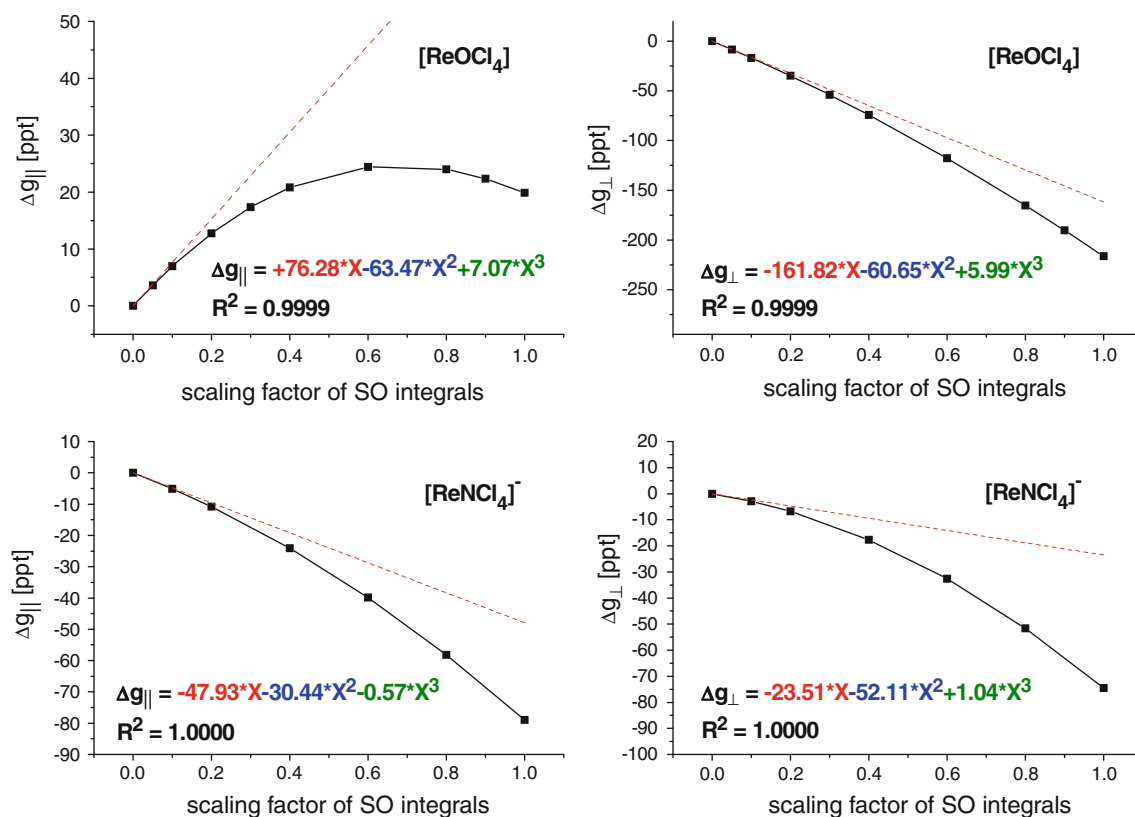

Fig. 4 Dependence of the g-shift tensor components in [Re^{VI}ECl$_4$]^q (E = O, N) complexes on the scaling of spin–orbit integrals. B3PW91 results at two-component DKH level. The *red dashed line* corresponds to the second-order perturbational treatment, which includes only first-order SOC effects
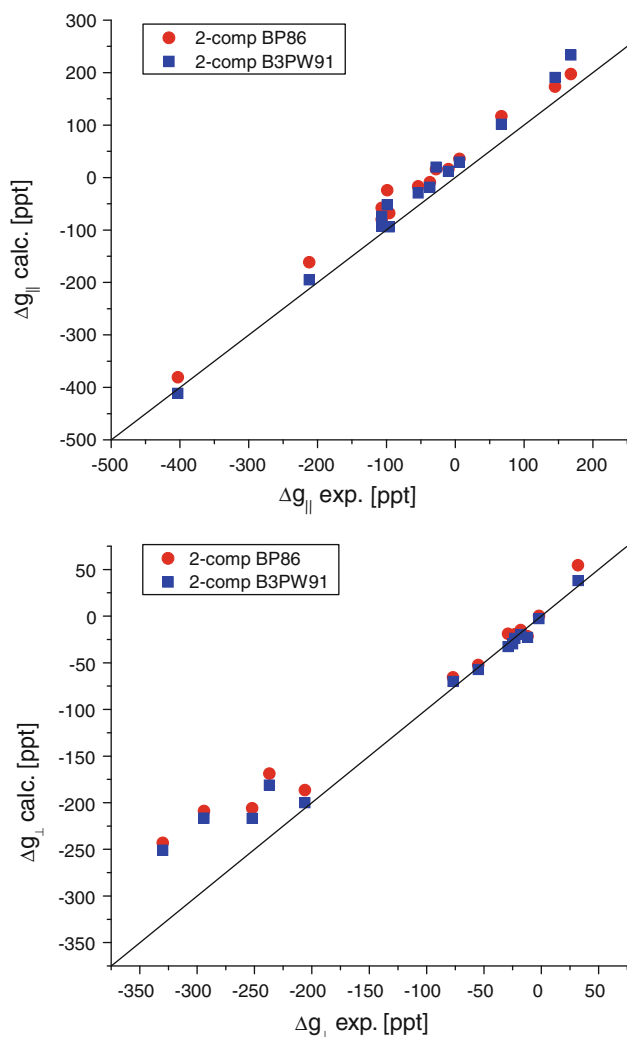
Fig. 5 Comparison of BP86 and B3PW91 two-component DKH g-shift results with experiment for the $[MOX_4]^q$ series

Table 2 Effect of the Hartree–Fock exact-exchange admixture on calculated g-tensors at the two-component DKH level

	$g_\parallel$ [ppt]	$g_\perp$ [ppt]	g_{iso} [ppt]
$[WOCl_4]^-$			
BP86	−161	−206	−191
B3PW91	−195	−217	−210
BPW91-30HF	−213	−222	−219
BPW91-40HF	−231	−228	−229
BPW91-50HF	−249	−233	−238
Exp.	−212	−252	−239
$[ReOCl_4]$			
BP86	16	−209	−134
B3PW91	20	−216	−138
BPW91-30HF	20	−220	−140
BPW91-40HF	18	−226	−144
BPW91-50HF	14	−232	−150
Exp.	−28	−294	−205

important than the functional for the reliable prediction of electronic g-tensors of heavier transition-metal complexes. In fact, the neglect of higher-order SOC contributions cannot be compensated by larger exact-exchange admixture even for $4d$ metal complexes.

The two- and four-component results do not match experiment perfectly for all complexes, even when using hybrid functionals at two-component level. While we cannot exclude that treatment of exchange and correlation leaves still some room for improvement, it seems more likely that neglect of environmental effects accounts for the remaining discrepancies (most of the complexes are anions, and significant interactions with the surroundings are expected).

Calculations on larger d^1 model complexes relevant to biological metal sites. The four-component mDKS module of ReSpect is based on a completely new integral code that is significantly more efficient than the integrals used so far

in other parts of ReSpect. In fact, for the non-hybrid functionals available so far in the four-component module (for which an RI is used, see Computational Details), we find the four-component calculations to be significantly faster than the previous two-component DKH implementation. This opens the way for fully relativistic DFT calculations of g-tensors (and other properties) for much larger systems than hitherto possible. Table 3 demonstrates this by comparing one- and four-component results for g-tensors of five larger complexes of V, Mo, and W (Fig. 1), which are relevant models of biological transition-metal sites. $[V(hidpa)_2]^{2-}$ is a realistic, close analog of amavadin, an unusual vanadium storage complex in certain mushrooms (see ref. [25] for more details and previous one-component calculations). The Mo(V) and W(V) complexes are spectroscopic and structural models for Mo and W redox enzymes. As for the smaller complexes of Tables 1 and 2, the inclusion of higher-order SOC effects renders all g-tensor components more negative and thus improves agreement with experiment. While, as expected, the higher-order SOC effects are more important for the Mo and particularly W complexes (cf. also Table 1), the magnitude of the higher-order SOC effects on the g-tensor of amavadin is also sizeable and clearly also improves the results. On a relative scale, the differences of four-component level compared to one-component level are indeed striking, leading to roughly 1.5 times as negative g-shift components for amavadin. Even if we keep in mind the overestimate of the SOC matrix elements in the four-component calculations by about 10% (see discussion above), the higher-order SOC contributions remain unexpectedly large. Part of the remaining discrepancies to experiment reflects the use of a GGA functional. As shown in ref. [25] at one-component

Table 3 Results for medium-sized d^1 complexes relevant to some metalloenzyme active sites

System	Method	Functional	Δg_{11} [ppt]	Δg_{22} [ppt]	Δg_{33} [ppt]	Δg_{iso} [ppt]
amavadin	DKH-1comp	BP86	−32	−10	−8	−17
		B3PW91	−48	−15	−13	−25
	mDKS-4comp	BP86	−46	−15	−13	−25
	Exp.[a]		−82	−20	−20	−41
$[MoO_2L^1]^-$	DKH-1comp	BP86	−136	−44	5	−58
		B3PW91	−195	−62	7	−83
	mDKS-4comp	BP86	−171	−65	−11	−82
	Exp.[b]		−192	−87	−16	−98
$[MoO_2L^2]^-$	DKH-1comp	BP86	−176	−52	3	−75
		B3PW91	−248	−71	4	−105
	mDKS-4comp	BP86	−227	−77	−16	−106
	Exp.[c]		−248	−105	−23	−125
$[MoS(Tp)\{S_2C_2(CO_2Me)_2\}]$	DKH-1comp	BP86	−81 (−57)	−18 (−11)	10 (12)	−30 (−19)
		B3PW91	−97 (−70)	−33 (−23)	2 (5)	−43 (−29)
	mDKS-4comp	BP86	−96 (−69)	−26 (−17)	2 (6)	−40 (−27)
	Exp.[c]		−76	−39	−32	−49
$[WS(Tp)\{S_2C_2(CO_2Me)_2\}]$	DKH-1comp	BP86	−211 (−154)	−64 (−45)	14 (27)	−87 (−57)
		B3PW91	−249 (−178)	−97 (−70)	−7 (12)	−118 (−79)
	mDKS-4comp	BP86	−257 (−186)	−108 (−79)	−37 (−2)	−134 (−89)
	Exp.[c]		−238	−122	−62	−141

Results obtained for experimental solid-state structures are given in parentheses

[a] Data taken from ref. [25]

[b] Data taken from ref. [6]

[c] Data taken from ref. [26]

level, inclusion of exact exchange in hybrid functionals renders particularly the g_{11} component still more negative, moving the result into the direction of the experimental value. From the results obtained here and in ref. [4], it seems reasonable to assume that we may to some extent view the effects of the functional and of higher-order SOC effects as roughly additive. Assuming such an additivity, taking into account the one-component hybrid functional results (cf. Table 3), and keeping in mind the slight overestimate of the SOC matrix elements at four-component level, already the modest exact-exchange admixture of the B3PW91 functional should bring relativistic theory and experiment almost into reasonable agreement. This contrasts with the conclusions of ref. [25], where somewhat larger exact-exchange admixtures have been assumed to be optimum (and a smaller importance of higher-order SOC had been assumed).

Similarly, the sizeable higher-order SOC effects obtained for the two molybdenum model complexes $[MoO_2L^1]^-$ and $[MoO_2L^2]^-$ alter the conclusions of ref. [5, 6] regarding the best-performing hybrid functional: assuming again additivity of the effects of functional and higher-order SOC, it appears that 20% HF exchange as exhibited by the B3PW91 functional would bring Δg_{22} and Δg_{33} into good agreement

with experiment, whereas the results for Δg_{11} would appear slightly too negative. Particularly, in the case of two dithiolene scorptionate complexes $[MS(Tp)\{S_2C_2(CO_2Me)_2\}]$ (M = Mo, W), the Δg_{11} component is too negative at the 4-component mDKS level. However, the bond lengths M=O, M–S, and M–N (M = Mo, W) optimized at the DFT level for all molybdenum and tungsten complexes considered here are somewhat longer compared to those determined by X-ray diffraction. A similar, but less pronounced, overestimation of the metal–ligand bond lengths was also found in our previous study [4]. Using the crystal structures for the two latter systems, the calculated Δg-shifts are reduced (cf. Table 1), leaving still some room for improvement of the four-component DFT results by using hybrid functionals. This demonstrates also the large sensitivity of the g-shifts in these systems to structure and the need of a good input structure.

4 Conclusions

Previous preliminary two-component Douglas–Kroll–Hess and four-component matrix Dirac–Kohn–Sham calculations of electronic g-tensors have been extended to (1) a

systematic validation and analysis for a series of group 5–7 $3d^1$, $4d^1$, and $5d^1$ transition-metal complexes and to (2) the first four-component DFT calculations on larger complexes of biological relevance with up to several tens of atoms. The latter results indicate that our recently developed four-component mDKS-RKB code does not only serve as a benchmark method, but it can also be used for routine applications of a fully relativistic DFT approach to more complex systems. The direct comparison of one-, two-, and four-component calculations within the same computer program, using identical functionals and basis sets, has allowed significant insights into the factors that contribute to the accuracy of these methods.

The advantage of multi-component relativistic approaches is the full inclusion of higher-order spin–orbit coupling (SOC) to all orders. Indeed, for all complexes studied here, sizeable higher-order SOC effects beyond leading order have been found, even for $3d$ complexes like amavadin. In particular for $4d$ and $5d$ complexes, second-order SOC contributions to g-shift tensor components tend to be on the same order of magnitude as the first-order terms (in one case even larger), and straightforward one-component calculations with leading-order perturbation theory thus give dramatic errors for such systems (even third-order SOC effects may be non-negligible). It turns out that, at least for the most of the present d^1 complexes, the higher-order SOC effects are significantly larger than the dependence of the results on the exchange–correlation functional. This unexpected result calls into question to some extent previous selections of "best functionals" for g-tensor calculations on transition-metal complexes, e.g., on biological transition-metal sites, which had assumed smaller relativistic effects.

References

1. Abragam A, Bleaney B (1970) Electron paramagnetic resonance of transition ions. Oxford Clarendon Press, Oxford
2. Harriman JE (1978) Theoretical foundations of electron spin resonance. Academic Press, New York
3. Kaupp M, Malkin VG, Bühl M (2004) Calculation of NMR and EPR parameters. Wiley-VCH, Weinheim
4. Hrobarik P, Malkina OL, Malkin VG, Kaupp M (2009) Chem Phys 356(1–3):229
5. Fritscher J, Hrobarik P, Kaupp M (2007) J Phys Chem B 111(17):4616
6. Fritscher J, Hrobarik P, Kaupp M (2007) Inorg Chem 46(20):8146
7. Hernandez-Marin E, Seth M, Ziegler T (2010) Inorg Chem 49(4):1566
8. Veloso-Bahamonde R, Ramirez-Tagle R, Arratia-Perez R (2010) Chem Phys Lett 491(4–6):214
9. Astashkin AV, Neese F, Raitsimring AM, Cooney JJA, Bultman E, Enemark JH (2005) J Am Chem Soc 127(47):16713
10. Schreckenbach G, Ziegler T (1998) Theor Chem Acc 99(2):71
11. Malkina OL, Vaara J, Schimmelpfennig B, Munzarova M, Malkin VG, Kaupp M (2000) J Am Chem Soc 122(38):9206
12. Neese F (2001) J Chem Phys 115(24):11080
13. Kaupp M, Reviakine R, Malkina OL, Arbuznikov A, Schimmelpfennig B, Malkin VG (2002) J Comput Chem 23(8):794
14. Rinkevicius Z, de Almeida KJ, Oprea CI, Vahtras O, Agren H, Ruud K (2008) J Chem Theory Comput 4(11):1810
15. Manninen P, Vaara J, Ruud K (2004) J Chem Phys 121(3):1258
16. Malkin I, Malkina OL, Malkin VG, Kaupp M (2005) J Chem Phys 123(24):244103
17. van Lenthe E, van der Avoird A, Wormer PES (1998) J Chem Phys 108(12):4783
18. Komorovsky S, Repisky M, Malkina OL, Malkin VG, Ondik IM, Kaupp M (2008) J Chem Phys 128(10):104101
19. Repisky M, Komorovsky S, Malkin E, Malkina OL, Malkin VG (2010) Chem Phys Lett 488(1–3):94
20. Hrobarik P, Hrobarikova V, Meier F, Repisky M, Komorovsky S, Kaupp M (2011) J Phys Chem A (in press)
21. TURBOMOLE (2009) version 6.0, a development of University of Karlsruhe and Forschungszentrum Karlsruhe GmbH
22. Eichkorn K, Weigend F, Treutler O, Ahlrichs R (1997) Theor Chem Acc 97(1–4):119
23. Andrae D, Haussermann U, Dolg M, Stoll H, Preuss H (1990) Theor Chim Acta 77(2):123
24. Schäfer A, Huber C, Ahlrichs R (1994) J Chem Phys 100(8):5829
25. Remenyi C, Munzarova ML, Kaupp M (2005) J Phys Chem B 109(9):4227
26. Sproules SA, Morgan HT, Doonan CJ, White JM, Young CG (2005) Dalton Trans (21):3552
27. Malkin VG, Malkina OL, Reviakine R, Arbuznikov AV, Kaupp M, Schimmelpfennig B, Malkin I, Repisky M, Komorovsky S, Hrobarik P, Malkin E, Helgaker T, Ruud K (2010) MAG-ReSpect, version 2.3
28. Repisky M (2009) Development and implementation of efficient relativistic methods for calculations of NMR and EPR parameters. Ph.D. Thesis, Bratislava
29. Becke AD (1988) Phys Rev A 38(6):3098
30. Perdew JP, Wang Y (1986) Phys Rev B 33:8822
31. Perdew JP, Wang Y (1986) Phys Rev B 34:7406
32. Becke AD (1993) J Chem Phys 98(2):1372
33. Becke AD (1993) J Chem Phys 98(7):5648
34. Perdew JP (1991) Phys B 172:1
35. Perdew JP, Wang Y (1992) Phys Rev B 45:13244
36. Hrobarik P, Reviakine R, Arbuznikov AV, Malkina OL, Malkin VG, Köhler FH, Kaupp M (2007) J Chem Phys 126(2):024107
37. Tsuchiya T, Abe M, Nakajima T, Hirao K (2001) J Chem Phys 115(10):4463
38. Kutzelnigg W, Fleischer U, Schindler M (1991) In: Diehl P, Fluck E, Günther H, Kosfeld R, Seelig J (eds) NMR basic principles and progress. Springer, Berlin
39. Schimmelpfennig B, AMFI (1996) Atomic spin-orbit mean-field integral program. Stockholms Universitet, Stockholm
40. Neyman KM, Ganyushin DI, Matveev AV, Nasluzov VA (2002) J Phys Chem A 106(19):5022
41. Jayatilaka D (1998) J Chem Phys 108(18):7587
42. Patchkovskii S, Ziegler T (1999) J Chem Phys 111(13):5730